ORNL--9702O863

C/Y1293-0178

CRADA FINAL REPORT
for
CRADA Number Y1293-0178

WELDING AND WELDABILITY OF DIRECTIONALLY SOLIDIFIED SINGLE CRYSTAL NICKEL-BASE SUPERALLOYS

J. M. Vitek, S. A. David, R. W. Reed
Oak Ridge National Laboratory

M. A. Burke and T. J. Fitzgerald
Westinghouse Electric Corporation

Date Published: September 1997

Prepared by the
Oak Ridge National Laboratory
Oak Ridge, Tennessee 37831
managed by
Lockheed Martin Energy Research Corporation
for the
U.S. Department of Energy
under contract DE-AC05-96OR22464

PROTECTED CRADA INFORMATION

This product contains Protected CRADA Information which was produced on November 30, 1997 under CRADA No. Y-1293-0178 and is not to be further disclosed for a period of five (5) years from the date it was produced except as expressly provided for in the CRADA.

DISCLAIMER

DISCLAIMER

Portions of this document may be illegible in electronic image products. Images are produced from the best available original document.

CONTENTS

ABSTRACT

Nickel-base superalloys are used extensively in high-temperature service applications, and in particular, in components of turbine engines. To improve high-temperature creep properties, these alloys are often used in the directionally-solidified or single-crystal form. The ability to weld these materials is highly desirable in that it would greatly facilitate component fabrication. Welding of these materials would also have the potential benefit of allowing for the repair of cracked or worn components. The objective of this CRADA project was to investigate the weldability of both experimental and commercial nickel-base superalloys in polycrystalline, directionally-solidified, and single-crystal forms. In addition to evaluating the weldability of nickel-base superalloys, the weld solidification microstructure was to be characterized to determine if the critical directionally-solidified or single-crystal microstructures in the base materials could be maintained in the welds.

The following conclusions were drawn from the results of this research program:

- Nickel-base superalloys in the polycrystalline form can be welded successfully under controlled conditions. IN625 is the preferred filler metal for welding.

- Directionally-solidified alloys can also be welded successfully under limited conditions. The directional nature of the base material is retained after welding.

- Single-crystal alloy CMSX4 is extremely vulnerable to cracking during welding. In addition, the single-crystal nature of the base material is lost after welding.

- Alloy rankings, in terms of overall weldability, were WSTC4 (best), CM247 and MarM002, and CMSX4 (worst).

- Weldability was found to correlate well with hot ductility measurements performed on a Gleeble™ thermo-mechanical simulator; good hot ductility corresponded to good weldability.

Research sponsored by the U. S. Department of Energy Defense Programs, Assistant Secretary, Technology Management Group, Technology Transfer Initiative under contract DE-AC05-96OR22464 with Lockheed Martin Energy Research Corporation.

OBJECTIVE

The objective of this CRADA project was to investigate the weldability of polycrystalline, directionally-solidified, and single-crystal, nickel-base superalloys. These materials are used extensively in turbine engine components. The ability to weld these materials is highly desirable in that it would greatly facilitate component fabrication. Welding of these materials would also have the potential benefit of allowing for the repair of cracked or worn components. Specifically, the program had four objectives:

1. to evaluate the weldability of nickel-base superalloys;
2. to characterize the solidification microstructure of the welds;
3. to evaluate the phase stability of the weldments during exposure to service conditions; and
4. to determine the mechanical properties of the welds.

Several of the objectives of this program were met. During the first stage of the investigation, in which the weldability of the nickel-base superalloys was investigated, it was found that these alloys are extremely susceptible to cracking during welding. As a result, the investigation concentrated on the cracking problem that was encountered, and its elimination. It was decided that a more thorough investigation of cracking behavior, evaluating the effect of alloy and weld process was warranted and this was carried out. Consequently, only limited work was performed on the phase stability activity (#3 above) and no mechanical property tests were performed. However, welds were produced to provide material for an extensive matrix of mechanical property tests that will be conducted by Westinghouse Electric Corporation after the termination of this CRADA.

BENEFIT TO DOE

Nickel-base superalloys are used extensively in turbine engines for both aircraft and land-based systems. The knowledge gained through this CRADA is valuable as far as learning what welding processes and methods may be available for use with these alloys, both for component fabrication as well as for component repair. The present study provides guidance for determining when, and if, welding can be incorporated into the manufacturing process. In addition, valuable experience with this class of materials has been gained. This experience with the welding of nickel-base superalloys can be applied to systems other than just turbine systems. For example, nickel-base superalloys are used extensively in the production of nuclear weapons and the expertise gained through this CRADA can be directly applied to the solution of problems that arise in these, and other, manufacturing enterprises.

TECHNICAL REPORT

INTRODUCTION

Nickel-base superalloys are attractive for turbine-engine applications because of their high-temperature strength and corrosion resistance. Particularly important for high temperature applications is the high-temperature creep resistance. In order to improve engine efficiency, there is a desire to increase the operating temperature range of turbine engines to higher temperatures. This has led to an evolution of nickel-base superalloys, from polycrystalline alloys to directionally-solidified alloys to single-crystal alloys. By aligning the grain structure with the stress axis, substantial improvements in high-temperature creep resistance were realized when directionally-solidified alloys replaced equiaxed, polycrystalline materials. Still further gains have been made when single-crystal alloys, without the presence of grain boundaries, were substituted for directionally-solidified materials. The elimination of grain boundaries, which contribute to high-temperature creep, has permitted the application of these alloys to still higher operating temperatures. Currently, engine parts are made up of all three types of materials.

Nickel-base superalloys are characterized by a two-phase mixture of cuboidal gamma prime (γ') precipitates in a solid-solution gamma (γ) matrix. The γ phase is face-centered cubic austenite while the γ' precipitate is a face-centered cubic phase based on the Ni_3Al composition. The γ' precipitate is present in large quantities, often in the range of 50 vol % or more. For alloys with grain boundaries (equiaxed polycrystalline, or directionally-solidified material), elemental additions are made to promote the formation of strengthening carbides at the grain boundaries. For single-crystal alloys, these carbides are not needed and the carbide-forming elements are not purposely added. Compositions and heat treatments are adjusted to avoid the formation of topologically close-packed phases such as σ, μ, and Laves phase.

Welding is an attractive method for fabricating turbine engine components. However, welding is not used extensively because of the vulnerability of nickel-base superalloys to hot-cracking. In addition, welding may critically alter the grain structure in these alloys, which may lead to poor performance. Nonetheless, welding is an attractive fabrication technology because it is economical. Furthermore, welding is potentially useful in component repair operations. It was the objective of this CRADA project to investigate the weldability of nickel-base superalloys, in both the directionally-solidified and single-crystal forms. Successful welding of these materials was then to be adapted into a commercially viable operation that could facilitate both component fabrication and repair.

EXPERIMENTAL PROCEDURE

Several different alloys were examined in this program. These included experimental alloys as well as commercial alloys. The experimental alloys (designated WSTC-x) were designed and processed by the Westinghouse Electric Corporation (WEC). Commercial alloys were obtained by WEC from commercial vendors. Each of these groups included alloys with the three

different grain structures: equiaxed polycrystalline, directionally-solidified, and single-crystal. The alloys and their compositions are listed in Table 1.

The alloys were examined in several conditions. A listing of the various heat treatments and the designations that are used throughout this report is given in Table 2. As-cast alloys were not subjected to any heat treatment following casting. Alloys in the solutionized condition were given a heat treatment at elevated temperature to reduce the as-cast inhomogeneity of the alloy. The exact heat treatment varied according to the specific alloy. Most alloys were given a solutionizing heat treatment followed by a precipitation heat treatment that was designed to achieve an optimum size and distribution of γ' precipitates. Often, the precipitation heat treatment was a two-step operation. The first step resulted in the primary precipitation of γ' and the second stage led to a secondary precipitation of finer γ'. A limited number of samples were given additional heat treatments to evaluate the effect of heat treatment on the cracking behavior. Extended homogenization treatments were conducted on some samples. In addition, a post-weld heat treatment was given to some alloys to assess the effect of heat treating after welding on the cracking behavior.

The alloys were investigated over a range of thicknesses. Thin sheet (0.030") specimens were used for many of the welding runs as well as for the Sigmajig testing[1]. The 0.030"-thick material was produced from thicker cast or heat-treated plate by electro-discharge machining. Thicker material (0.125 and 0.25") was also used in order to evaluate the effect of sample thickness on welding behavior. Welding of thick plate (0.8") as well as rod material (0.85" diam) was carried out for making stock material for mechanical property test specimens.

Several welding processes were used in the course of this study: laser welding, electron beam welding, gas-tungsten-arc (GTA) welding, and plasma-arc welding (PAW). A range of welding conditions were examined for each process. Some of the welds were autogenous welds, in which the base material was melted and re-solidified without the addition of any filler metal. In other cases, filler metal was used. Often, rather than using filler metal in the form of wire additions, a shim of suitable composition (another nickel-base superalloy) was inserted between the two pieces to be joined and, in this way, the weld was a mixture of the filler-metal composition and the base-metal composition.

A Gleeble™ thermo-mechanical simulator was used to carry out hot ductility tests. Small tensile specimens, 1.5" long, were machined from sheet stock (0.030" thick) of the base material and tested during heating or cooling. Typically, the sample was heated to a peak temperature of approximately 1330°C and then cooled to a specific temperature where the strength and ductility were measured. This test procedure was repeated over a range of final temperatures to assess the hot ductility as a function of temperature.

The Sigmajig weldability test was used initially to assess the weldability of the alloys[1]. In this type of test, the sample, in the form of a sheet tensile sample, is loaded in tension and then a weld bead is made over the material. The load is varied from test to test and the threshold stress at which cracking occurs is taken as a measure of the weldability of the alloy. As will be shown later, this test was of minimal value in this program because of the orientation and nature of the cracking. In subsequent work, weld cracking behavior was evaluated by examination of the surface of welded samples. Dye penetrant was also used on occasion to aid in the detection of cracks. Metallographic analysis was employed for more detailed evaluation of the cracking

behavior, including the detection of sub-surface cracks and fine cracks in both the fusion and heat-affected zones (HAZ), as a function of welding conditions and alloy composition. Cracks were identified on samples in the as-polished condition. The degree of cracking, both in terms of the size of cracks as well as the number of cracks that were observed, was taken as a measure of the weldability of the alloys. This analysis proved to be more meaningful than the Sigmajig testing procedure.

Metallography was also used to evaluate the microstructure of the various welded samples. Optical metallography was performed on polished and mounted samples in both the as-polished and the etched condition. The etchant that was used was Modified Marble's Reagent (25 ml H_2O, 25 ml alcohol, 50 ml HCl, 10 gm cupric sulphate). Supplementary metallographic analysis was conducted with the use of scanning electron microscopy, transmission electron microscopy, and electron microprobe analysis. X-ray diffraction was used to measure the grain structure texture.

Residual stresses were evaluated by means of hole-drilling experiments. Strain gages were mounted on as-cast slabs and stresses were measured as holes were drilled into the slab. The hole drilling caused a relief of the residual stresses in the castings and these changes in the stress state were followed with the strain gages.

RESULTS

Weldability

The first round of experiments consisted of preliminary weldability tests on experimental alloys as well as selected commercial alloys. Autogenous melt runs were made at various speeds (5 to 35 "/min) on thin sheet (0.030") using the gas-tungsten-arc (GTA) and pulsed-laser processes. The tendency to form surface cracks was monitored visually and the results are presented in Tables 3 and 4. The entire class of alloys were prone to cracking in the form of centerline cracks, or transverse cracks, or both. For the GTA welds, less cracking was evident as the welding speed was reduced. Typical micrographs showing the absence of cracks at low speeds and the presence of transverse cracks at high speeds for alloy CM247CC are shown in Figure 1. Also, for the WSTC-4 alloy, the heat-treated alloy showed a significantly greater resistance to cracking compared to the alloy in the as-cast condition. This improved resistance to cracking corresponded to a marked decrease in the alloy inhomogeneity, as shown in Figure 2. The WSTC-4 and CM247 alloys showed the best weldability when using the GTA process. In general, the pulsed laser welding led to a marked improvement in weldability compared to the GTA welds. For all alloys except the IN738LC, there were some conditions where no cracking was found after pulsed laser welding. Furthermore, for most alloys, no surface cracking was found at any speed (5 "/min to 30 "/min).

The preliminary tests were followed by Sigmajig testing to assess the fusion zone (or weld metal) cracking behavior in a more quantitative manner. These tests were carried out by applying a tensile load on the samples and then welding normal to the stress axis. Tests were repeated at increasing load levels. The threshold stress level at which cracking first appeared, and when failure occurred, was recorded. The results are presented in Table 5. The CM247DS alloy

showed complete failure at a very low threshold stress. All the other alloys that were tested failed at relatively high stresses. However, in all of these cases, early cracking was detected at lower stress levels. In many cases, the cracking was transverse to the weld, and therefore parallel to the stress axis. Under these conditions, the Sigmajig test is not meaningful since cracking along the stress axis does not promote complete failure to a significant degree. Therefore, it was concluded that the Sigmajig testing for weldability was an inappropriate test for these alloys and welding conditions, and further testing was discontinued.

Following the first round of weldability tests, it was determined that the directionally-solidified MarM002 and the single-crystal CMSX4 alloys were of most interest for evaluating the potential of welding in commercial practice. Therefore, a second round of weldability tests was conducted on these two alloys only. A broader range of welding procedures was used, and welds were performed on a range of sample thicknesses, from 0.030" sheet to 0.125 and 0.25" thick plate. For thick samples (0.125 and 0.25"), pulsed laser welds were of insufficient power to achieve full penetration. Therefore, the laser welds were made with a continuous-wave (CW) laser system. In addition, electron-beam (EB), GTA, and plasma-arc welding (PAW) processes were examined. The results of the welding tests are presented in Tables 6-9. The effect of welding orientation was also examined in the second round, with welds made parallel or perpendicular to the crystal growth direction.

As was found in the preliminary results (Table 3), the MarM002 sheet welds cracked at all welding speeds. In contrast, the thicker MarM002 material showed some resistance to weld cracking. At the lower speeds, there were no surface cracks found, while at the fastest welding speed, transverse cracks were detected.

The CW laser welding results (Table 7) were different from those for pulsed laser welding (Table 4). The window in which no surface cracking was found was smaller for CW laser welding for both the CMSX4 and MarM002 alloys. Repeated welding runs confirmed this tendency. The results in Table 7 also show that the welding direction has little influence on the cracking behavior. For the 0.030" thick MarM002, marginally more cracking was found when welding transverse to the growth direction. For CW laser welding, the thicker MarM002 material (0.125 or 0.25") showed more vulnerability to cracking than the thin (0.030") material. This is directly opposite to the behavior found for the GTA welds as a function of sample thickness. The CMSX4 material was found to have surface cracks at all thicknesses, and at all speeds. This is in agreement with the preliminary pulsed laser weld results which showed the CMSX4 alloy to be more vulnerable to weld cracking.

The results from EB welding are shown in Table 8. As was the case for laser welding, the CMSX4 alloy was less resistant to cracking than the MarM002 alloy. In fact, all conditions tested showed cracking in CMSX4. For the MarM002 alloy, the cracking behavior as a function of sample thickness was similar to the behavior found for GTA welds, with the thicker material being more resistant to cracking. In fact, there was no cracking found in the EB welds at all but the highest welding speed while the thinner sheet material cracked at all speeds. As noted above, this is contrary to the results for the laser welding (Table 7).

PAW welding results are given in Table 9. PAW welding was only done on the thicker samples since it is not an appropriate technique for thin gage material. All PAW welds were made at a welding speed of 10 "/min. All of the PAW welds showed surface cracking, regardless of

alloy (CMSX4 or MarM002) or weld direction (parallel or transverse to the growth direction).

A limited number of welds were made on cylindrical samples of CMSX4 and MarM002 (diameter 0.75 and 0.85", respectively) with a high-power (9 KW) laser welding system. The welds were made over a range of speeds from 10 to 150 "/min. These tests were conducted to determine if a keyhole mode during laser welding, which is possible with the high-power system, would affect the cracking behavior. The welds showed severe cracking for both alloys and under all conditions.

The effect of filler metal additions on the welding behavior was first examined by machining a groove in the base material and then using a filler metal to make the final weld. A limited number of tests were conducted. The base metal was MarM002 in all cases, and three different filler metal additions were examined: IN625, MarM002, and CMSX4. The GTA welding process was used. For the welds with IN625 and MarM002 filler metal additions, no surface cracks were found. However, the welds with CMSX4 filler metal additions showed surface cracks. This is in agreement with the autogenous weld results which showed the CMSX4 alloy was consistently more prone to cracking than the MarM002 alloy.

Another series of welds were made to investigate the nature of plug welds, in which a plug made of suitable material was welded into a hole in the base metal. This process is of possible commercial value in making repairs on as-cast material. The plugs were 1/4" long and 3/16" in diameter and the base metal holes were 3/16" in diameter and 3/4" long. Circumferential welds were made after force-fitting the plug in the holes; no filler metal additions were used. Two different base metals were used, CMSX4 and MarM002, while three different plug materials were examined, IN625, MarM002 and CMSX4. Four welding processes were employed: CW laser, PAW, GTA, and EB welding. The results are presented in Table 10. All welds with the MarM002 base metal and IN625 plug were found to be free of cracks, regardless of the welding process. In contrast, all of the welds with MarM002 or CMSX4 plugs on MarM002 base metal showed surface cracks.

The welding behavior for thick-plate butt welds was also examined. Various combinations of parameters were studied to identify the best conditions for producing thick-plate butt welds for mechanical property specimens. The welds were made using the EB welding process. Based on the earlier results (Tables 6-9), the EB welding process showed the greatest promise for producing crack-free welds in thicker plate. Also, welds with IN625 filler metal additions showed the greatest potential for being crack-free. Two sample configurations were examined. The first was a butt joint between two 3/4-inch plates with thin "filler metal" shims of IN625 between the plates. The second configuration used butt joints of cylindrical samples of 0.8" diameter with the same IN625 filler metal shims. The cylindrical specimens were machined from both sides to a final thickness of 0.4" in the region to be welded so as to reduce the curvature of the rod specimens and produce a more uniform specimen thickness.

The results are presented in Table 11. It was found that a shim width of 0.040" was optimal, based on overall weld appearance. The welds with the IN625 filler metal showed little evidence of surface cracking. More detailed metallographic examination of the transverse-view cross sections revealed that cracking within the fusion zone was, in general, not present.

~~*** Protected CRADA Information, as marked. ***~~

However, small cracks were found in the HAZ. These cracks were often irregular and difficult to identify; multiple metallographic sections were often examined to obtain conclusive results. Furthermore, the small cracks were not readily observed in etched samples so the metallographic sections were often examined in the unetched condition. The effects of welding orientation, homogenization treatment, and pre- and post-weld heating were examined as well. Small cracks on the order of 0.02" were found in all samples. These cracks were found to originate in the HAZ and, when the cracking was more severe, they extended into the fusion zone. The cracks were along grain boundaries as well as along segregated zones within the grains of the MarM002. In all cases, the cracks were aligned along the growth direction of the material. The welding orientation did not have a significant effect on the tendency to form cracks, in agreement with earlier results (Tables 7-9). Typical micrographs are shown in Figure 3. The total crack length of all observed cracks as a function of welding condition is plotted in Figure 4. From this plot no clear effect of increased homogenization treatment, sample size, pre- and post-weld heating, or post weld heat treating emerges. No combination of conditions completely eliminated cracking. However, the use of pre- and post-weld heating kept the cracking propensity to a minimum. Therefore, multiple plates and rods for producing stock material for mechanical property testing were welded using the pre- and post-weld heating. The mechanical property test samples were prepared during this CRADA study and were supplied to WEC but there was insufficient time to carry out the tests.

Finally, tests were run to evaluate the potential of cladding material with a welding process. A 1/16 inch plate of cladding was placed on the base material of the same width and length and a defocussed electron beam was slowly scanned over the material, producing a molten puddle along the way. Different combinations of cladding and base material were selected . This procedure was not evaluated in detail but the preliminary results showed the cladding to be intact, with the cladding grain structure aligned with the base material grain structure.

Hot Ductility

Hot ductility testing was performed on the Gleeble™ thermo-mechanical simulator following either heating or cooling. Typically, the sample was heated to a peak temperature of approximately 1330°C (just below the liquidus temperature) and then cooled to a fixed temperature at which point the ductility was measured by pulling the sample in tension. Hot ductility tests were performed on the WSTC-4 alloy, in both the as-cast and HT conditions, on CMSX4 in the as-cast condition, on CM247CC and CM247DS in the as-cast condition, and on MarM002 in the HT-1 and HT-2 conditions. The hot ductility tests provided information on how rapidly the strength and ductility are recovered when cooling from the nil strength temperature.

Results for alloy WSTC-4, in both conditions, are shown in Figure 5. It can be seen that this alloy, in the as-cast condition, has very low ductility at elevated temperatures. In contrast, in the heat treated condition, the ductility recovery is much more dramatic. Significantly, the hot strength increased as well as the hot ductility after heat treating. Compared to the WSTC-4 alloy in the HT condition, the hot ductilities for CMSX4, CM247, and MarM002 were noticeably reduced. A comparison is shown in Figure 6. The poor hot ductility can be directly correlated with the welding behavior and the tendency to form cracks. As shown in Table 3, WSTC-4 in the as-cast condition was prone to cracking when welded, but in the HT condition, it was resistant to

cracking. The susceptibility to cracking corresponded to a poor hot ductility. This correlation between reduced hot ductility and increased cracking susceptibility also held true for the other alloys. Compared to WSTC-4 in the HT condition, all the other alloys (CMSX4, CM247, and MarM002) showed a greater tendency to crack when welded and they also exhibited poorer hot ductility. Therefore, the hot ductility test seems to be a reasonable gage for the welding behavior of these alloys in terms of the resistance to cracking during welding.

As-Welded Grain Structure

When welding single-crystal or directionally-solidified material, a critical feature of the weld is the grain structure. In the case of directionally-solidified base material, it is important for the weld grain structure to have the same preferred grain orientation as that in the base material. Similarly, for single-crystal materials, it is desirable for the weld grain structure to maintain the single crystal nature of the base material. Otherwise, the properties of the weldment may not be adequate.

The grain structure of welds made on directionally-solidified material was investigated in order to assess the range of orientations present in the weld, and to compare this with the range found in the base metal. X-ray measurements were made and a texture analysis was performed. The welds were on the CM247DS material, in the HT-1 condition. The range of orientations of the growth axes in the base material was approximately ±10°. GTA welds, with welding speeds of 5, 10, and 35 "/min, were examined. It was found that the range of grain orientations were comparable to those found in the base material. In fact, the range was somewhat smaller in the welds but this difference is not considered to be significant. Therefore, it was concluded that for the directionally-solidified material the welding procedure did not introduce any more scatter in crystal orientation than what was already present in the base metal.

The situation for single-crystal welds was not as promising in terms of grain structure. In general, single crystal welds show distinct dendritic growth zones that result from the selection of optimally oriented dendritic growth directions[2]. Even with the presence of these different dendritic growth zones, the single crystal nature of the weld can, in principle, be maintained. However, for nickel-base single-crystal welds, there is a strong tendency to form stray crystals, which are new grains with random orientations[3,4]. This tendency was also found in the present study. An example of stray crystal formation is shown in Figure 7.

Microstructure

Only limited work was carried out to evaluate the microstructure, by means of optical microscopy, electron microprobe measurements and transmission electron microscopy. As shown in Figure 2, the as-cast material was quite inhomogeneous. For the WSTC4 alloy, a homogenization treatment considerably reduced the degree of inhomogeneity (see Figure 2). The as-cast inhomogeneity was much more difficult to eliminate in the CMSX4 alloy. Figure 9 shows the CMSX4 material in the as-cast and solutioned conditions. After heat treating, the compositional fluctuations across the dendrites are reduced but the interdendritic constituents remain. The presence of these interdendritic precipitates is likely to be undesirable since the HAZ cracks propagated along these interdendritic zones (see Figure 3). Based on earlier work[3], it is expected that the large interdendritic phase is γ'. These γ' particles are considerably larger than

those that form following solutioning and aging heat treatments and they result from solute partitioning during the solidification process[3]. The large interdendritic precipitates were not found in welds[5] but their presence in the HAZ is sufficient to cause cracking.

Residual Stresses

A hole drilling method was used to evaluate the residual stresses in as-cast slabs of WSTC-4 and CMSX4. The slabs were 2.5×4×0.5" (WSTC-4) and 3×6×0.375" (CMSX4) in size. Residual stress was measured as a function of depth, up to a depth of nearly 0.1". Measurements were made on the as-cast surfaces as well as on surfaces that were lightly machined to provide a smooth surface. Measurements were made at the corners of the castings as well as in the center of the slabs. In nearly all cases, the stresses were within the range of ±10 ksi, far below the yield strengths of these materials. Beyond a depth of 0.05", the residual stresses typically fell within a range of ±5 ksi. The maximum residual stress was reached in the WSTC-4 casting, with a value of +13 ksi. In general, the residual stresses in the WSTC-4 alloy exceeded those for the CMSX4. Representative plots showing the residual stress as a function of depth in the CMSX4, taken at the slab corner, are shown in Figure 8. Based on these results, it was concluded that the residual stresses were minor and further measurements were not conducted.

DISCUSSION

The primary objective of this program was to assess the weldability of nickel-base alloys that are used for components in turbine engines. The results have shown that this class of alloys is very prone to the formation of weld cracks. However, the investigation has shown that under some conditions, acceptable welds are achievable. The optimum conditions vary from process to process, as is clearly shown in Tables 3 through 11, and what may be optimum for one welding process is not necessarily desirable for another. Some of the more important parameters that have a consistent and predictable effect on weldability are discussed below. In addition, the consequences of this investigation in terms of potential applications of welding to component manufacture and repair are discussed.

The alloy heat treatment prior to welding is one of the primary parameters that affects weldability. In perhaps the clearest example, the weldability of alloy WSTC4 improved from poor to excellent for thin sheet GTA welds when the alloy was homogenized after casting (see Table 3). This trend was supported by quite a bit of additional evidence. First, for those welds in which HAZ cracking was found, the cracks were often associated with the second phase constituents as shown in Figure 3. Secondly, the CMSX4 alloy, which showed significant interdendritic precipitation in the as-cast condition, was the alloy that was most prone to weld cracking. Furthermore, a homogenization treatment for this alloy did not eliminate its tendency to form cracks or the presence of the interdendritic precipitates. This is not surprising since the CMSX4 alloy contains rhenium additions that are included specifically to slow down diffusion kinetics. While this is a desirable feature of the alloy in terms of improving its high temperature creep rate, the retention of the solidification segregation is clearly a drawback in terms of weldability. The present results suggest that an improved homogenization treatment, that produces a more

homogenous microstructure, would be far more desirable in terms of avoiding weld cracks and such a homogeneous microstructure may also still be resistant to high temperature creep because of its innately slow diffusion kinetics. Further evidence for the value of achieving a homogenous microstructure has been found in a recent investigation of alloy PWA1480, another nickel base superalloy used in turbine engine components[3,4]. In that study, the extensive cracking in the weld metal was associated with interdendritic precipitates that remained after homogenization. Finally, in those welds where IN625 was used as a filler metal, fusion zone cracking was avoided in many cases but cracking could not be avoided in the HAZ. Once again, the HAZ cracks were associated with second phase constituents in the base material that prevailed even after normal homogenization. The current results clearly show that a homogenized microstructure is preferred as far as weldability is concerned. It is also likely that truly homogenized microstructures would be beneficial in terms of high temperature mechanical properties, although this is conjecture at this time.

Fusion zone cracking was a problem in many of the alloys and under different conditions. CMSX4 was vulnerable to fusion zone cracking in nearly all cases, while the same cracking tendency was much reduced in alloy WSTC4, and even in alloys CM247 and MarM002 under certain conditions. However, the results consistently showed that the addition of IN625 as a filler metal was desirable in that it eliminated the tendency for fusion zone cracks. Thus, the present results indicate that the use of IN625 as a filler metal is desirable. It is likely that much of the success in avoiding fusion cracks with IN625 filler metal can be attributed to the presence of grain boundary strengtheners in this alloy. Thus, the grain boundaries that form in the fusion zone are somewhat protected from cracking because of the presence of these strengtheners. This conclusion is supported by similar studies on alloy PWA1480 where fusion zone cracking was most often associated with grain boundaries[3,4]. The PWA1480 is intended for use in the single crystal form and it does not have grain boundary strengthener additions. Thus, the grain boundaries that existed in the fusion zone microstructure were especially weak and vulnerable to cracking.

This study has also shown that hot ductility is a good measure of an alloy's vulnerability to weld cracking. The hot ductility test measures both the hot strength and the hot ductility. The results showed that alloys with poor hot strength and/or hot ductility were vulnerable to weld cracking. Thus, the hot ductility test may be a suitable and convenient screening test for evaluating the weld behavior of candidate alloys.

The grain structure characterization in this program has important implications. The results showed that the directional character of grains in directionally solidified alloys can be maintained in the welds. Therefore, it is reasonable to assume that the welds in these materials may have comparable properties to the directionally solidified base material. The same cannot be said for single crystal welds. For these materials, the single crystal nature of the alloy is likely to be lost in the fusion zone. Given the fact that these alloys do not have specific additions to the improve the strength of grain boundaries (there is no need for these additions in the base material because there are no grain boundaries), one can reasonably assume that the fusion zone of these alloys is noticeably weaker than the base material. This conclusion is supported by the fact that the CMSX4 alloy, which is designed for use as a single crystal, showed the worst welding behavior. Thus, if welding is to be considered for this class of alloy, either of two solutions must

be employed. One alternative is to use filler metal compositions with grain boundary strengtheners. This in fact was done when IN625 filler metal was used and the fusion zone cracking was eliminated. However, it is likely that the fusion zone will be weaker than the base material as is observed when the two alloys are compared in their base material conditions. The second alternative is to devise welding procedures that avoid the formation of stray crystals in the fusion zone. Some suggestions that might help avoid the stray crystal formation have been made in a recent paper[3], but the complete elimination of stray crystals is likely to be a difficult task.

The mechanical properties of the weldments were not tested in this program. However, welds were made to yield material that was appropriate for testing and this material was shipped to WEC for examination at a later time.

CONCLUSION

This CRADA program between ORNL and Westinghouse Electric Corporation has provided valuable information on the weldability of nickel-base superalloys in the form of polycrystalline, directionally solidified, or single crystal material. Much needed insight into the possibilities for using welding as a fabrication tool for turbine engine components made of these nickel-base superalloys has been gained. The conclusions of this study are the following:

1) Polycrystalline nickel-base superalloys can be welded under controlled conditions. The welding conditions (speed, material thickness) are dependent upon the welding process that is employed. IN625 is the preferred filler metal for welding.

2) Directionally solidified nickel base superalloys can also be welded successfully, under limited conditions. Once again, IN625 is the preferred filler metal alloy. The grain structure in the welded material is comparable to that in the directionally solidified base material.

3) Single crystal alloy CMSX4 was found to be vulnerable to cracking for all conditions and all processes that were explored. In addition, the welded single crystal material grain structure was undesirable in that the fusion zone microstructure was no longer single crystal in nature.

4) The ranking of alloys, in terms of overall weldability, was:

WSTC4 (best)
CM247 and MarM002
CMSX4 (worst).

Furthermore, the CM247 was found to be marginally better than the MarM002 alloy.

5) The weldability of the different alloys, and in different heat-treated conditions, correlated well with the hot ductility. Alloys or heat treatments that led to improved hot ductility also led to improved resistance to weld cracking. Therefore, hot ductility may be an excellent screening test for weldability.

REFERENCES

1. G. M. Goodwin, "Development of a New Hot-Cracking Test - The Sigmajig," Welding Journal, 66(2), 33s-38s, 1987.

2. M. Rappaz, S. A. David, J. M. Vitek, and L. A. Boatner, "Analysis of Solidification Microstructures in Fe-Ni-Cr Single-Crystal Welds," Metall. Trans. A, 21A, 1767-1782, 1990.

3. J. M. Vitek, S. A. David, and L. A. Boatner, "Microstructural Development in Single Crystal Nickel Base Superalloy Welds," to appear in Sci. and Technol. of Welding and Joining, 2(3), 1997.

4. S. A. David, J. M. Vitek, S. S. Babu, L. A. Boatner, and R. W. Reed, "Welding of Nickel Base Superalloy Single Crystals," Sci. and Technol. of Welding and Joining, 2(2), 79-88, 1997.

5. S. S. Babu, S. A. David, J. M. Vitek and M. K. Miller, "Atom-Probe Field-Ion Microscopy Investigation of CMSX-4 Ni-Base Superalloy Laser Beam Welds," J. Physique IV, Vol. 6, Colloq. C5, C5-253 - C5-258, 1996.

INVENTIONS

No inventions were made or reported as part of the work on this CRADA.

ASSESSMENT OF COMMERCIALIZATION POSSIBILITIES

In general, the results from this study show that the nickel-base superalloys are extremely vulnerable to cracking. However, conditions under which acceptable welds can be produced have been identified for some alloy combinations. This information can be incorporated into commercial practice. For service conditions where directionally-oriented grains are acceptable, welding may provide a simple and cost-effective alternative to current component fabrication. In addition, the studies have shown that weld repair of these materials is also feasible. More work is required to ascertain the potential of welding in the fabrication of single-crystal nickel-base superalloy components. However, even for these materials, which are exceptionally prone to cracking and to loss of their single crystal nature, valuable insight has been gained as to what factors need to be addressed in order to achieve acceptable welds.

PLANS FOR FUTURE COLLABORATION

This CRADA has already led to additional collaborative work between Westinghouse Electric Corporation and Lockheed-Martin. A work-for-others program has been implemented between the Westinghouse Turbine Systems Division and ORNL. Westinghouse Electric Corporation has also expressed interest in extending this CRADA. Currently, other avenues of funding are being examined as means for further collaborative work.

Table 1: Nominal Compositions of Alloys That Were Examined.

Alloy Designation	Grain Structure*	Composition (wt %)																
		Ni	Cr	Co	Al	Ti	Nb	Ta	Mo	W	Zr	B	C	Hf	Re	Mn	Fe	Si
WSTC-1	SC	proprietary composition																
WSTC-4	SC	proprietary composition																
WSTC-6	SC	proprietary composition																
WSTC-7	SC	proprietary composition																
IN738LC	PC	61.5	16.0	8.5	3.4	3.4	0.9	1.8	1.8	2.6	0.1	0.01	0.11					
CM247CC	PC	63.2	8.0	9.0	5.5	0.8	0.1	3.2	0.6	9.5			0.08					
CM247DS	DS	63.2	8.0	9.0	5.5	0.8	0.1	3.2	0.6	9.5			0.08					
CMSX4	SC	60.7	6.4	9.6	5.7	1.1		6.5	0.6	6.4				0.1	2.9			
MarM002	DS	61.1	9.0	10.0	5.5	1.5		2.5	0.2	10.0	0.04	0.01	0.15					
IN625	PC	60.1	21.5	0.2	0.2	0.3	3.7 (Nb+Ta)		8.9				0.04			0.3	4.5	0.2

* PC - polycrystalline
DS - directionally solidified
SC - single crystal

Table 2: Alloy Heat Treatment Conditions

Alloy	Designation	Heat Treatment*
WSTC (all)	as cast	none
WSTC (all)	HT	solution and precipitation heat-treated
CM247	as cast	none
CM247	HT-1	solution heat-treated
CM247	HT-2	HIP + solution and precipitation heat-treated
MarM002	HT-1	HIP + solution heat-treated
MarM002	HT-2	HIP + solution and precipitation heat-treated
CMSX4	as cast	none
CMSX4	HT	multi-step solutionizing heat treatment as specified by manufacturer
IN738	HT	as-received in commercial heat-treated condition; details unavailable
IN625	HT	commercial heat-treated condition

* HIP - hot isostatically pressed

Table 3: Autogenous GTA Welding Results
(thin sheet, 0.030")

Alloy	Condition	Welding Speed		
		5"/min	10"/min	35"/min
CMSX4	as cast	N	C	C, T
CMSX4	as cast + pre-heat	C, T	C, T	T
CMSX4	HT	C	C, T	C, T
CMSX4	HT + pre-heat	C	C	C
CM247CC	HT-1	N	N	T
CM247DS	HT-1	N	N	T
CM247DS	HT-1 + pre-heat		C	C
WSTC-4	as cast	C	C	C, T
WSTC-4	HT	N	N	N
WSTC-7	HT	C	C, T	T
IN738LC	HT	C, T	C, T	T
MarM002	HT-1	C	C	C
MarM002	HT-1 + pre-heat			C
MarM002	HT-2	C	C	C
MarM002	HT-2 + pre-heat	C	C	C

C = Centerline cracking
T = Transverse cracking
N = No cracking

~~*** Protected CRADA Information, as marked. ***~~

Table 4: Autogenous Pulsed Laser Welding Results
(thin sheet, 0.030")

Alloy	Condition	Welding Speed			
		5"/min	10"/min	15"/min	30"/min
CMSX4	as cast	N	N	T	T
CMSX4	HT	-	-	-	-
CM247CC	HT-1	N	N	N	N
CM247DS	HT-2	N	N	N	N
WSTC-4	as cast	N	N	N	N
WSTC-4	HT	N	N	N	N
WSTC-7	HT	N	N	N	N
IN738LC	HT	T	T	T	T
MarM002	HT-1	N	N	N	N
MarM002	HT-2	N	N	N	GBC

C = Centerline cracking
T = Transverse cracking
N = No cracking
GBC = Grain Boundary Cracking

~~*** Protected CRADA Information, as marked. ***~~

Table 5: Sigmajig Test Results

Alloy	Sigmajig Test Results as a Function of Tensile Stress
CMSX4 (as cast)	0 ksi centerline cracking
	10 ksi transverse cracking
	20-25 ksi transverse and centerline cracking
	30 ksi complete failure
CM247CC (HT-1)	0-9 ksi no cracking
	12-20 ksi centerline cracking
	30 ksi complete failure
CM247DS (HT-2)	0 ksi no cracking
	2 ksi centerline cracking
	5 ksi complete failure
WSTC-4 (As cast)	0 ksi centerline cracking
	15-38 ksi transverse cracking
	40 ksi complete failure
WSTC-4 (HT)	0-25 ksi no cracking
	30-35 ksi centerline cracking
WSTC-7 (HT)	0 ksi centerline and transverse cracking
	10 ksi no cracking
	12 ksi centerline and transverse cracking
	15 ksi complete failure
IN738 (HT)	0 ksi centerline and transverse cracking
	20-30 ksi, 45 ksi no cracking
	35-40 ksi transverse cracking

Table 6: Autogenous GTA Welds
(variable thickness)

Alloy	Thickness (inches)	Welding Speed		
		5"/min	10"/min	35"/min
MarM002	0.125	N	N	T
MarM002	0.030	C	C	C

C = Centerline cracking
T = Transverse cracking
N = No cracking

~~*** Protected CRADA Information, as marked ***~~

Table 7: Autogenous CW Laser Welding Results
(variable thickness)

Alloy	Condition	Weld Direction	Thickness (inches)	Welding Speed			
				5"/min	10"/min	15"/min	30"/min
CMSX4	as cast	∥	0.030	T	C, T	T	T
CMSX4	as cast	∥	0.25	C, T	C, T	C, T	C, T
MarM002	HT-1	∥	0.030	N	N	N	N
MarM002	HT-1	⊥	0.030	N	T	T	T
MarM002	HT-1	∥	0.125	C, T	C, T	T	T
MarM002	HT-1	⊥	0.125	C, T	C, T	T	T
MarM002	HT-1	∥	0.25	C	C	C	C, T
MarM002	HT-1	⊥	0.25	C, T	C, T	C, T	C, T

∥ = Parallel to growth direction
⊥ = Perpendicular to growth direction

C = Centerline cracking
T = Transverse cracking
N = No cracking

~~*** Protected CRADA Information, as marked. ***~~

Table 8: Autogenous EB Welding Results
(variable thickness)

Alloy	Condition	Thickness (inches)	Welding Speed			
			5"/min	10"/min	15"/min	30"/min
CMSX4	as cast	0.25	C, T	C, T	T	T
MarM002	HT-1	0.030	C	C	C	C
MarM002	HT-1	0.125	N	N	N	N
MarM002	HT-1	0.25	N	N	N	T

C = Centerline cracking
T = Transverse cracking
N = No cracking

***~~Protected CRADA Information, as marked.~~ ***

Table 9: Autogenous PAW Welding Results
(variable thickness, all welds at 10"/min)

Alloy	Condition	Weld Direction	Thickness (inches)	Welding Speeds
MarM002	HT-1	∥	.25	C
MarM002	HT-1	⊥	.25	T
CMSX4	HT	∥	.25	T
CMSX4	HT	⊥	.25	T

∥ = Parallel to growth direction
⊥ = Perpendicular to growth direction
C = Centerline cracking
T = Transverse cracking

~~*** Protected CRADA Information, as marked. ***~~

Table 10: Hole Plugging Results
(1/4" long, 3/16" diam. plug in 3/16" diam hole)

base material	plug material	Welding Process			
		CW laser	PAW	GTA	EB
MarM002	IN625	no cracks	no cracks	no cracks	no cracks
MarM002	MarM002	surface cracks	surface cracks	surface cracks	surface cracks
MarM002	CM247	crater cracks	crater cracks	crater cracks	surface cracks

~~*** Protected CRADA Information, as marked. ***~~

Table 11: Results from EB Butt Welds

Material Combination	ID Fig. 4	Plate Thickness (inches)	Filler Shim Thickness (inches)	Process Conditions	Remarks/Results
MarM002/MarM002		0.4		EB, 30 "/min	transverse surface cracks
MarM002/MarM002		0.4		EB, 20 "/min	transverse surface cracks
MarM002/IN625/MarM002		0.4	0.020	EB, 20 "/min	cracking
MarM002/IN625/MarM002		0.4	0.040	EB, 10 "/min	cracks at fusion line
MarM002/MarM002		0.75		EB, 10 "/min	transverse cracks
MarM002/IN625/MarM002		0.75	0.040	EB, 7 "/min	no surface cracks
MarM002/IN625/MarM002		0.75	0.060	EB, 7 "/min	no surface cracks, HAZ cracks
MarM002/IN625/MarM002		0.75	0.040	EB, 7"/min	HAZ cracks
MarM002/IN625/MarM002		0.75	0.020	EB, 17"/min	HAZ cracks
MarM002/IN625/MarM002	A	0.75	0.040	EB, 20"/min	full size plate, perpendicular to growth direction, no surface cracks
MarM002/IN625/MarM002	A	0.75	0.040	EB, 20"/min	full size plate, parallel to growth direction, no surface cracks
MarM002/IN625/MarM002	B	0.75	0.040	EB, 10"/min	with pre and post heat, no cracks initially but HAZ cracks in mounted sample

Table 11: Results from EB Butt Welds (contd.)

MarM002/IN625/MarM002	C	0.75	0.040	EB, 10"/min	additional homogenization at 1235°C/6h, no cracks initially but HAZ cracks in mounted sample
MarM002/IN625/MarM002	C	0.75	0.040	EB, 10"/min	(repeat) additional homogenization at 1235°C/6h, no cracks initially but HAZ cracks in mounted sample
MarM002/IN625/MarM002	C	0.75	0.040	EB, 10"/min	(repeat) additional homogenization at 1235°C/6h, no cracks initially but HAZ cracks in mounted sample
MarM002/IN625/MarM002	D	0.75	0.040	EB, 10"/min	additional homogenization at 1235°C/6h, perpendicular to growth direction, HAZ cracks
MarM002/IN625/MarM002	D	0.75	0.040	EB, 10"/min	additional homogenization at 1235°C/6h, parallel to growth direction, HAZ cracks
MarM002/IN625/MarM002	G	0.75	0.040	EB, 10"/min	additional double homogenization at 1235°C/12h plus pre- and post-weld heat treat, perpendicular to growth direction, HAZ cracks
MarM002/IN625/MarM002	E	0.4	0.040	EB, 10"/min	rod, additional double homogenization at 1235°C/12h, perpendicular to growth direction, HAZ cracks
MarM002/IN625/MarM002	F	0.4	0.040	EB, 10"/min	rod, additional double homogenization at 1235°C/12h plus pre- and post-weld heat treat, perpendicular to growth direction, HAZ cracks
MarM002/IN625/MarM002	H	0.75	0.040	EB, 10"/min	additional double homogenization at 1235°C/12h plus post-weld heat treat, HAZ cracks

~~*** Protected CRADA Information, as marked. ***~~

FIGURE CAPTIONS

Figure 1 Top surface optical micrographs of autogenous GTA welds of alloy CM247CC showing (a) the absence of cracks when welded at low speed (10"/min) and (b) the presence of cracks when welded at higher speeds (35"/min).

Figure 2 Optical micrographs of alloy WSTC-4 in the (a) as-cast condition and the (b) heat treated condition. The large interdendritic precipitates (likely γ') dissolve during homogenization and re-precipitate during heat treating in the form of much finer precipitates.

Figure 3 Typical transverse section optical micrographs of MarM002 welds showing the cracking in the HAZ and the occasional extension of these cracks into the fusion zone. (a) standard heat treatment condition showing cracks following the interdendritic contours, (b) heat treated material with additional pre- and post-weld heating also showing the crack propagation along the interdendritic zones and extending into the fusion zone, (c) extended solution heat treatment and pre- and post-weld heating.

Figure 4 Plot showing the total crack length in MarM002 GTA butt welds with IN625 filler metal for various material conditions (see Table 11). Multiple bars for any given condition represent multiple measurements on different metallographic samples.

Figure 5 Hot ductility measurements (reduction in area) upon cooling for alloy WSTC-4 in the (a) as-cast and the (b) heat treated conditions.

Figure 6 Comparison of hot ductility measurements (upon cooling) for various alloys: (a) heat treated WSTC-4, (b) as-cast CMSX4, (c) heat treated CMSX4, (d) heat treated CM247DS, (e) heat treated CM247CC, (f) solutioned MarM002 (HT-1), (g) solutioned and aged MarM002 (HT-2).

Figure 7 Fusion zone interface in a GTA weld on alloy CM247DS. The growth direction in the HAZ is aligned with the weld direction (vertical) and hence the HAZ along the interface is a single crystal. The growth of stray crystals in the fusion zone with different orientations is apparent.

Figure 8 Plot of residual stress measured by hole drilling as a function of depth in as-cast CMSX4.

Figure 9 Optical micrographs of CMSX4 base material in the (a) as-cast and (b) heat treated conditions. The large interdendritic precipitates (likely to be γ') that form during solidification are still present after heat treating.

a)

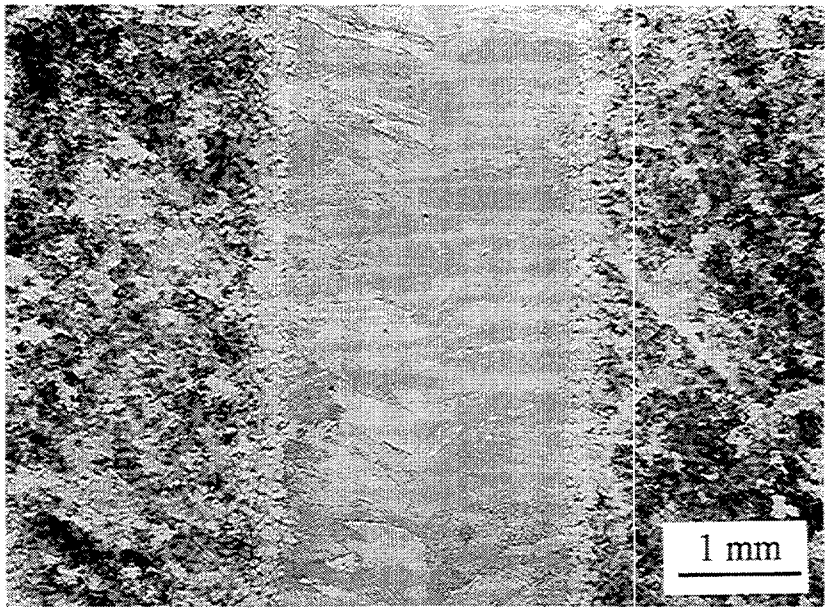

b)

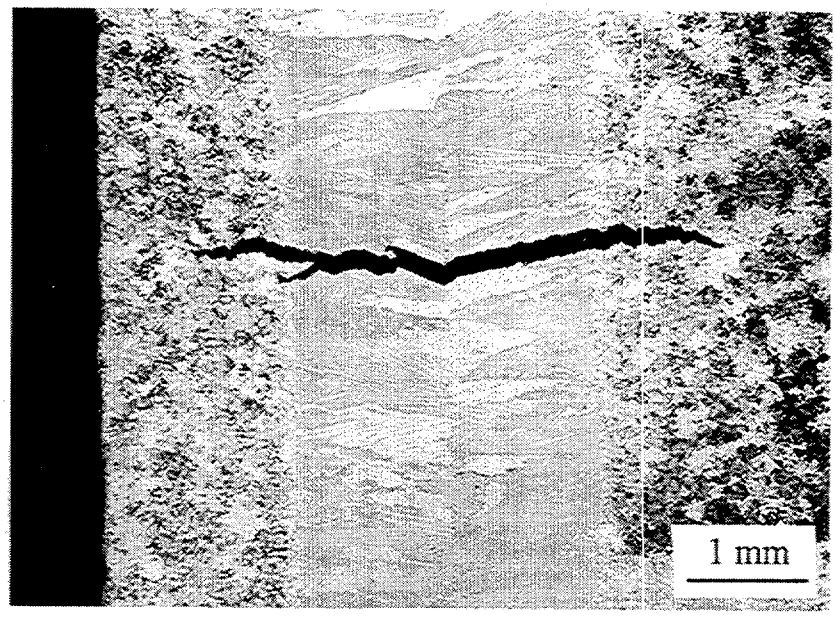

Figure 1: Top surface optical micrographs of autogenous GTA welds of alloy CM247CC showing (a) the absence of cracks when welded at low speed (10"/min) and (b) the presence of cracks when welded at higher speeds (35"/min).

a)

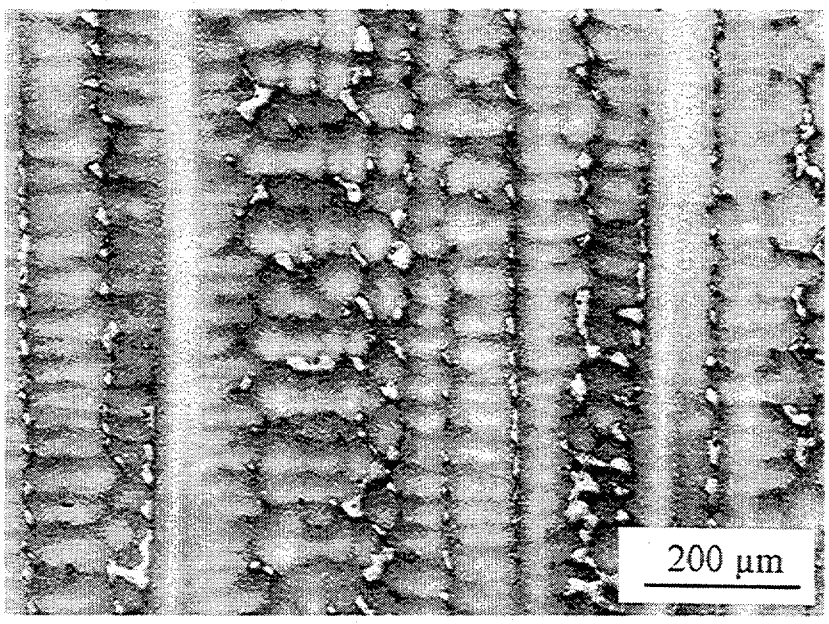

b)

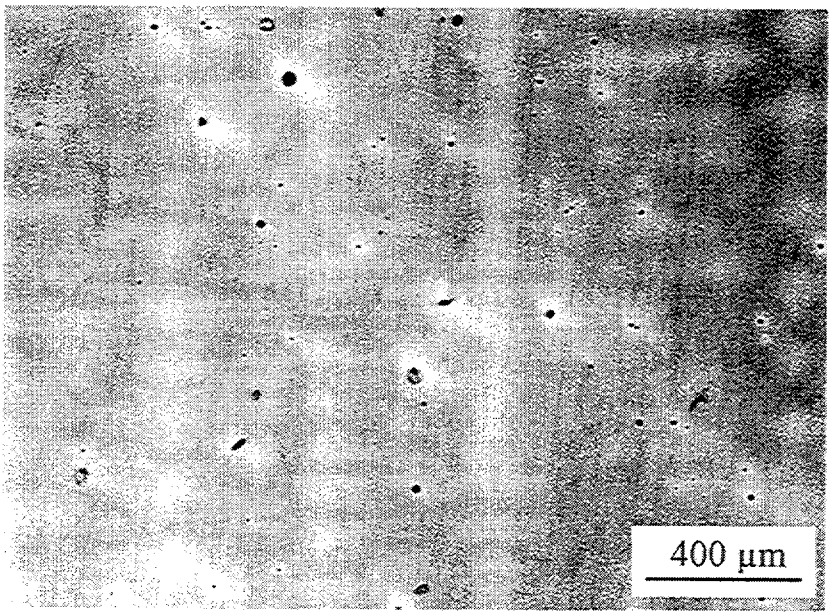

Figure 2: Optical micrographs of alloy WSTC-4 in the (a) as-cast condition and the (b) heat treated condition. The large interdendritic precipitates (likely γ') dissolve during homogenization and re-precipitate during heat treating in the form of much finer precipitates.

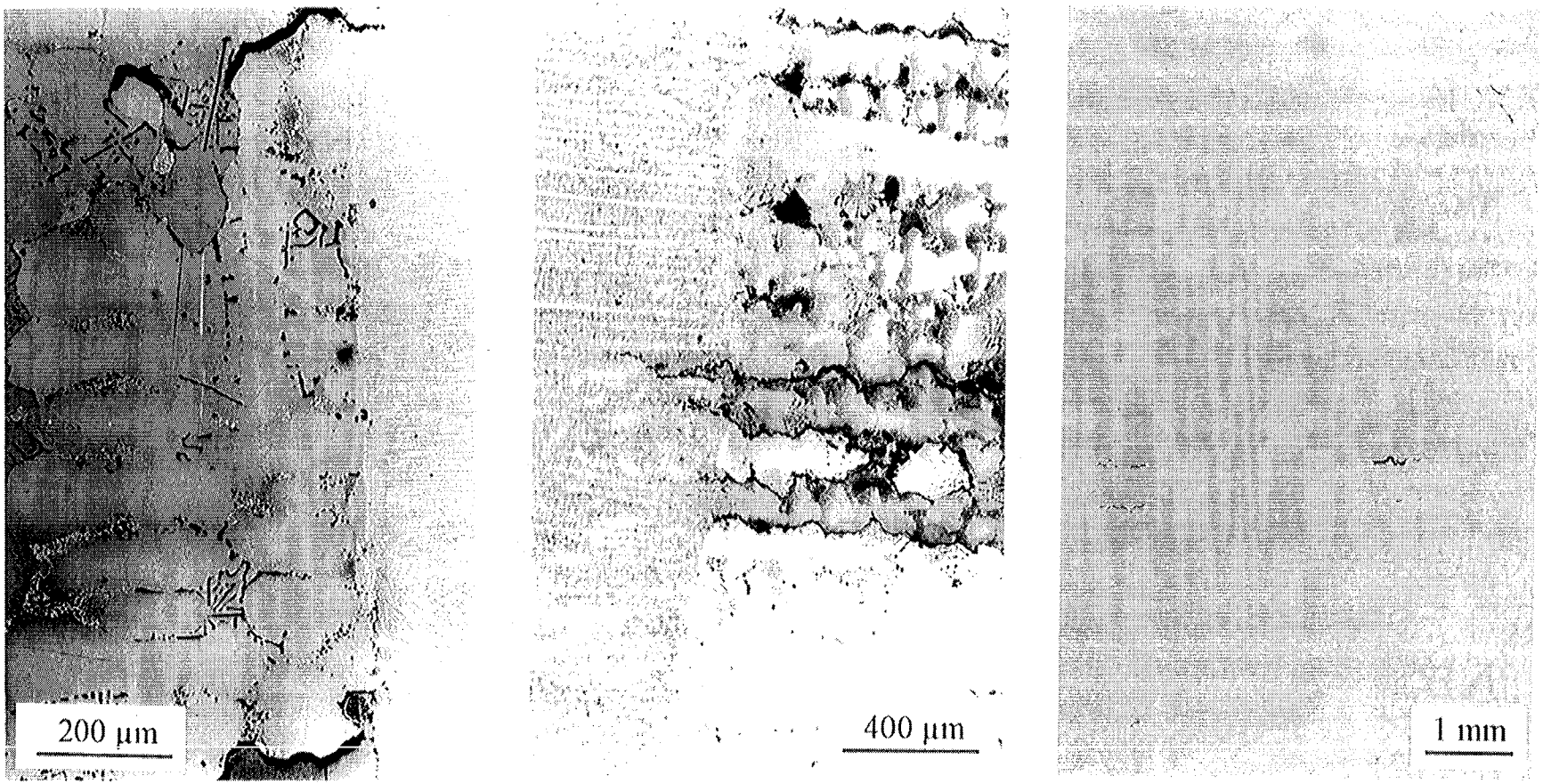

Figure 3: Typical transverse section optical micrographs of MarM002 welds showing the cracking in the HAZ and the occasional extension of these cracks into the fusion zone. (a) standard heat treatment condition showing cracks following the interdendritic contours, (b) heat treated material with additional pre- and post-weld heating also showing the crack propagation along the interdendritic zones and extending into the fusion zone, (c) extended solution heat treatment and pre- and post-weld heating.

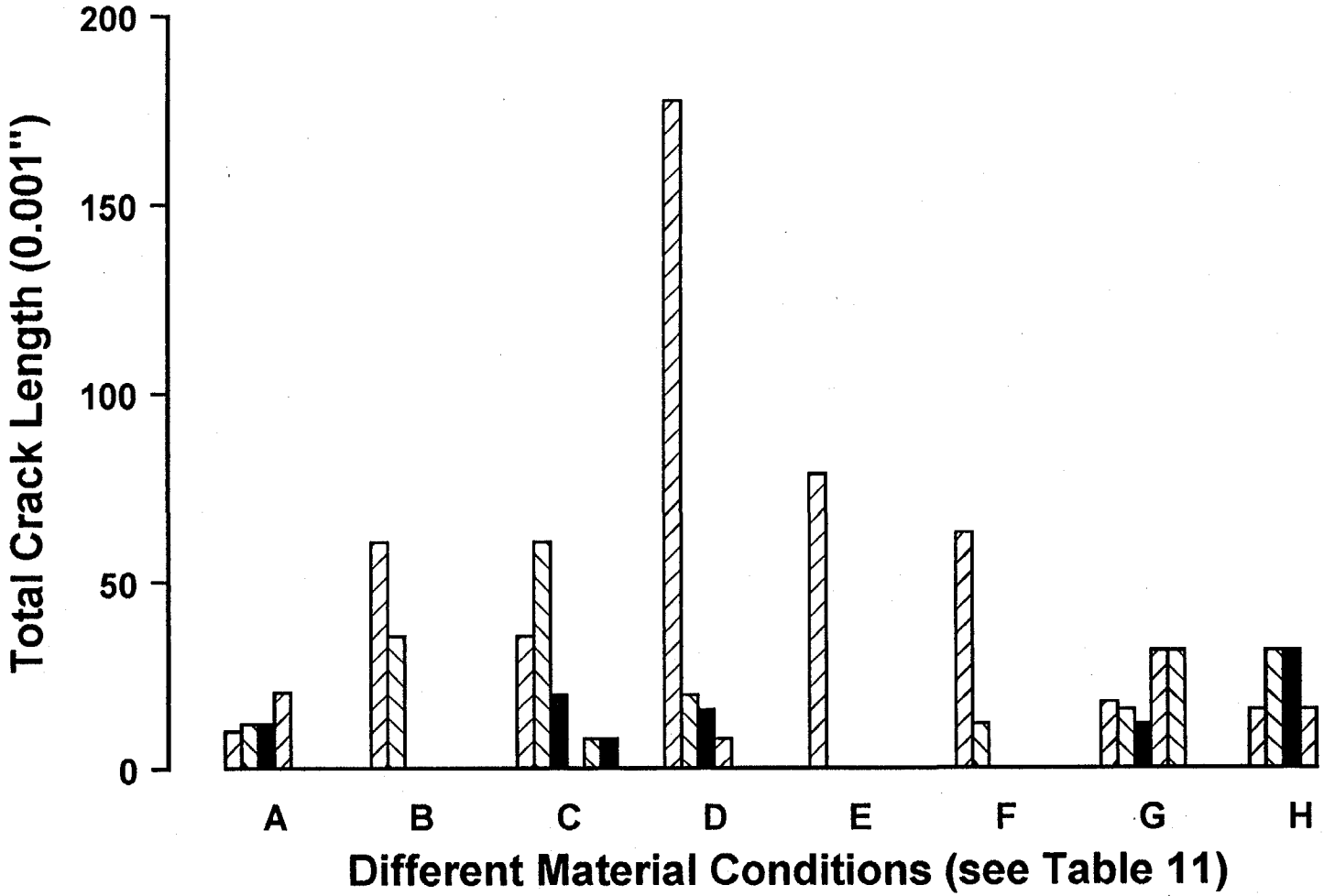

Figure 4: Plot showing the total crack length in MarM002 GTA butt welds with IN625 filler metal for various material conditions (see Table 11). Multiple bars for any given condition represent multiple measurements on different metallographic samples.

*** ~~Protected CRADA Information, as marked~~. ***

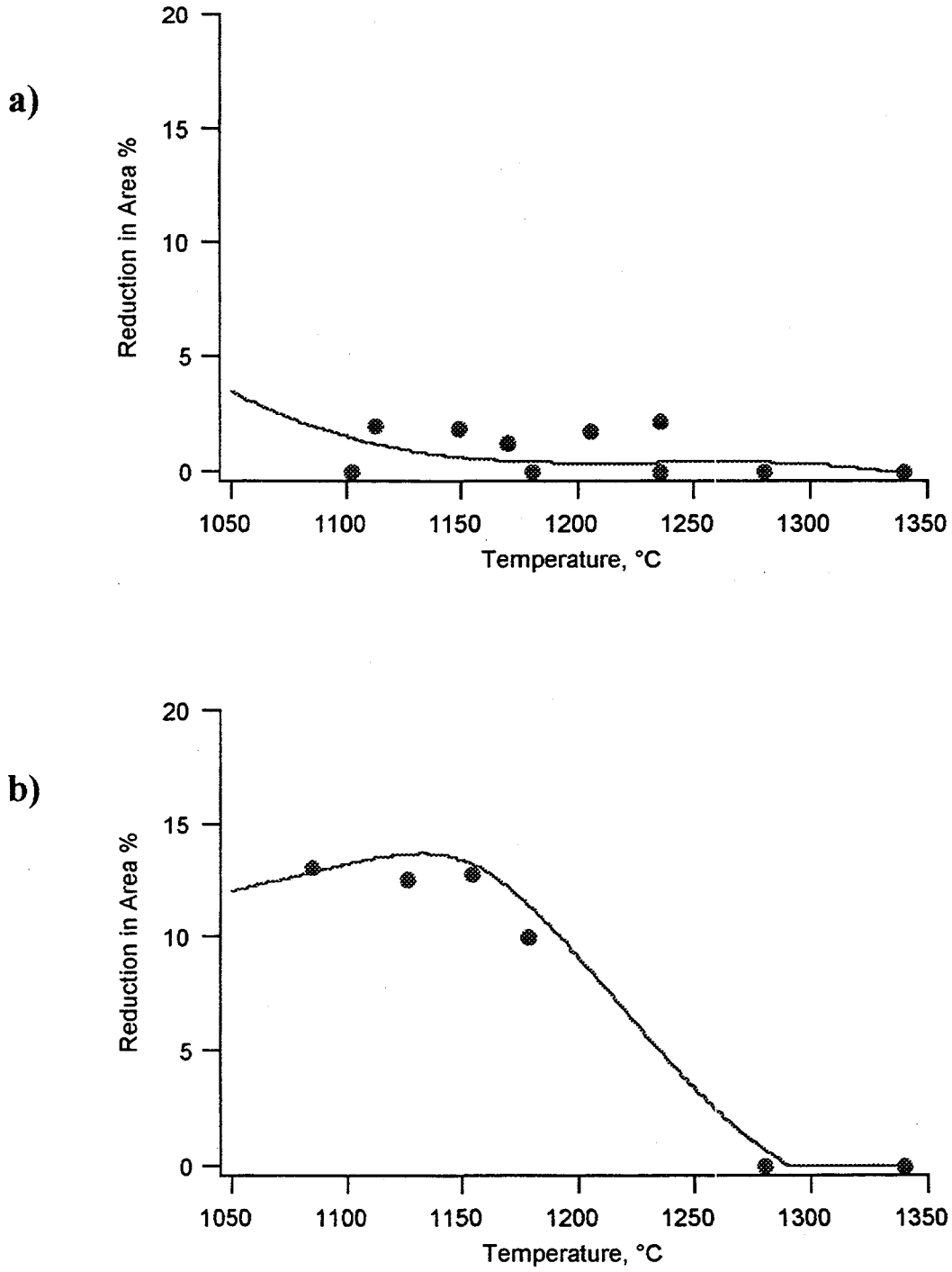

Figure 5: Hot ductility measurements (reduction in area) upon cooling for alloy WSTC-4 in the (a) as-cast and the (b) heat treated conditions.

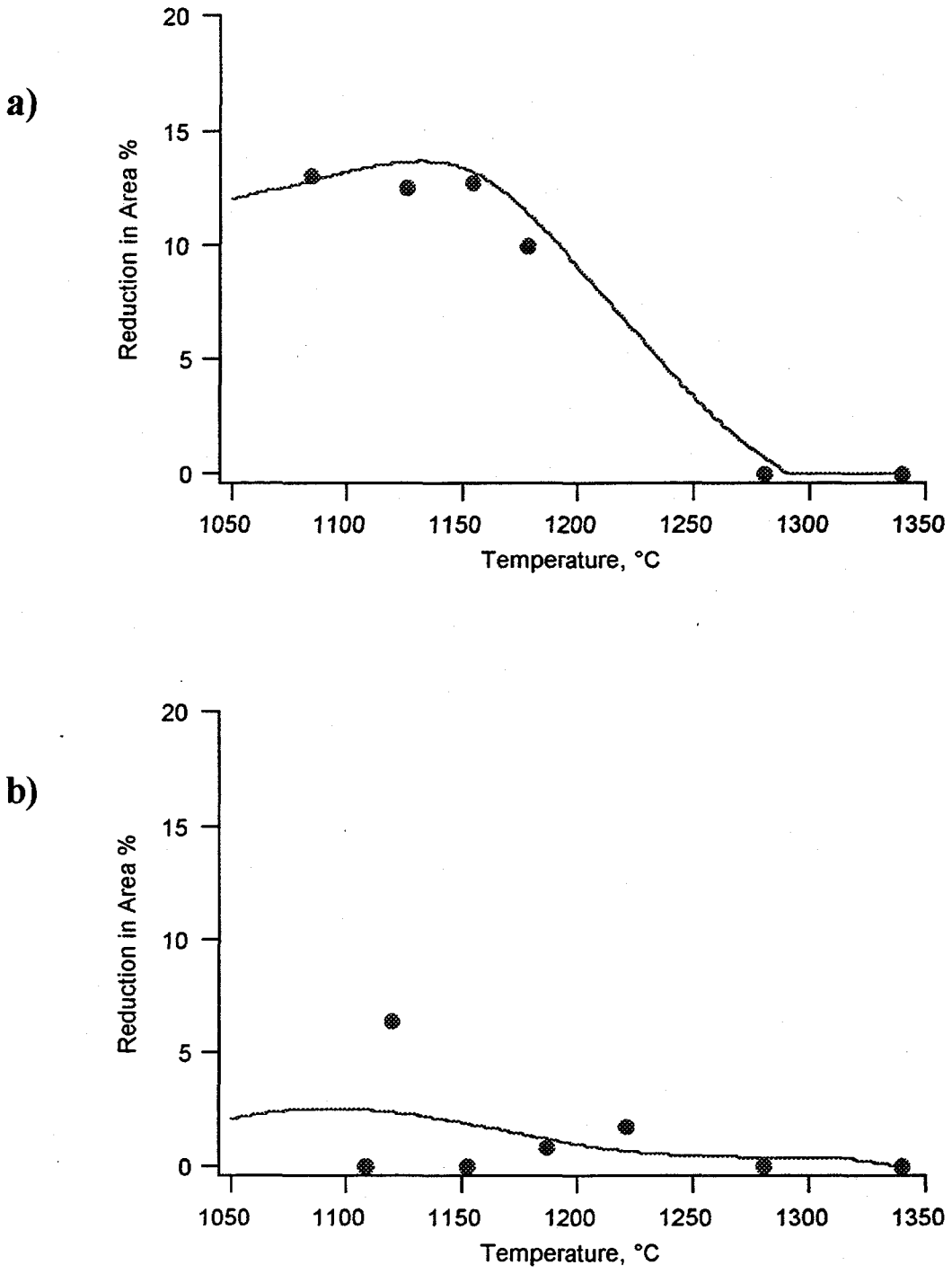

Figure 6: Comparison of hot ductility measurements (upon cooling) for various alloys: (a) heat treated WSTC-4, (b) as-cast CMSX4, (c) heat treated CMSX4, (d) heat treated CM247DS, (e) heat treated CM247CC, (f) solutioned MarM002 (HT-1), (g) solutioned and aged MarM002 (HT-2).

c)

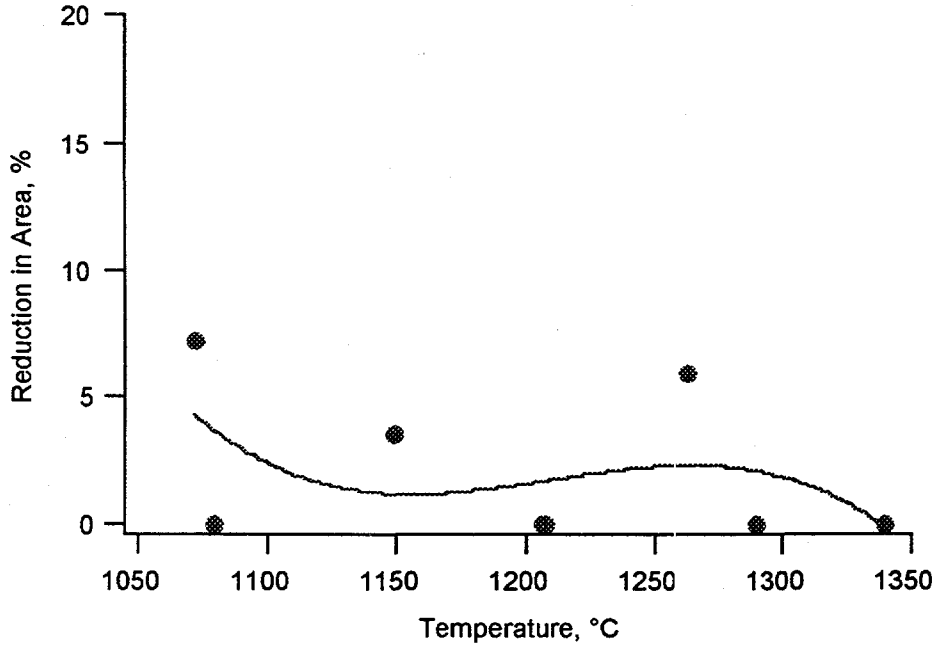

d)

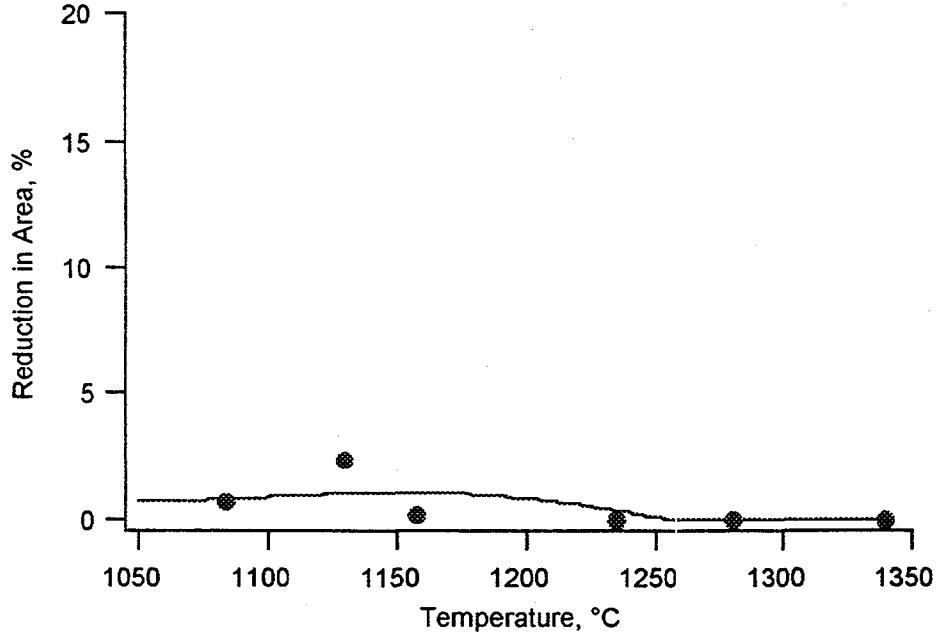

Figure 6 (contd.): Comparison of hot ductility measurements (upon cooling) for various alloys: (a) heat treated WSTC-4, (b) as-cast CMSX4, (c) heat treated CMSX4, (d) heat treated CM247DS, (e) heat treated CM247CC, (f) solutioned MarM002 (HT-1), (g) solutioned and aged MarM002 (HT-2).

e)

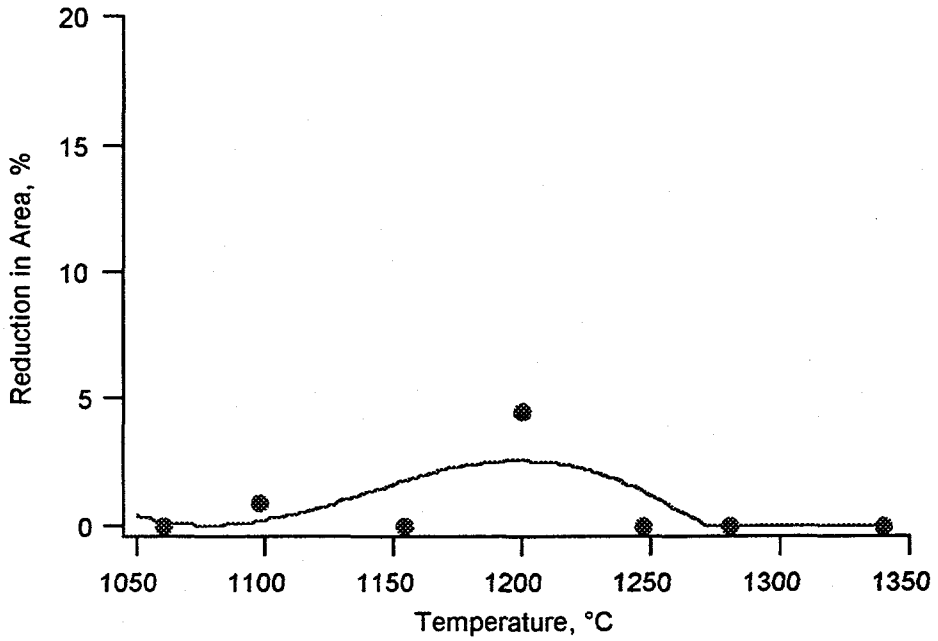

f)

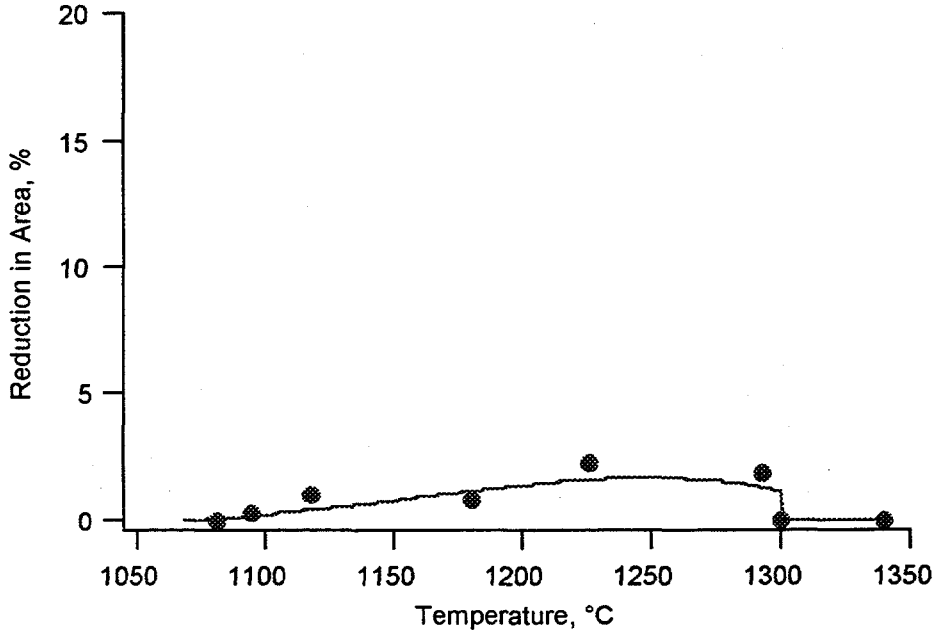

Figure 6 (contd.): Comparison of hot ductility measurements (upon cooling) for various alloys: (a) heat treated WSTC-4, (b) as-cast CMSX4, (c) heat treated CMSX4, (d) heat treated CM247DS, (e) heat treated CM247CC, (f) solutioned MarM002 (HT-1), (g) solutioned and aged MarM002 (HT-2).

g)

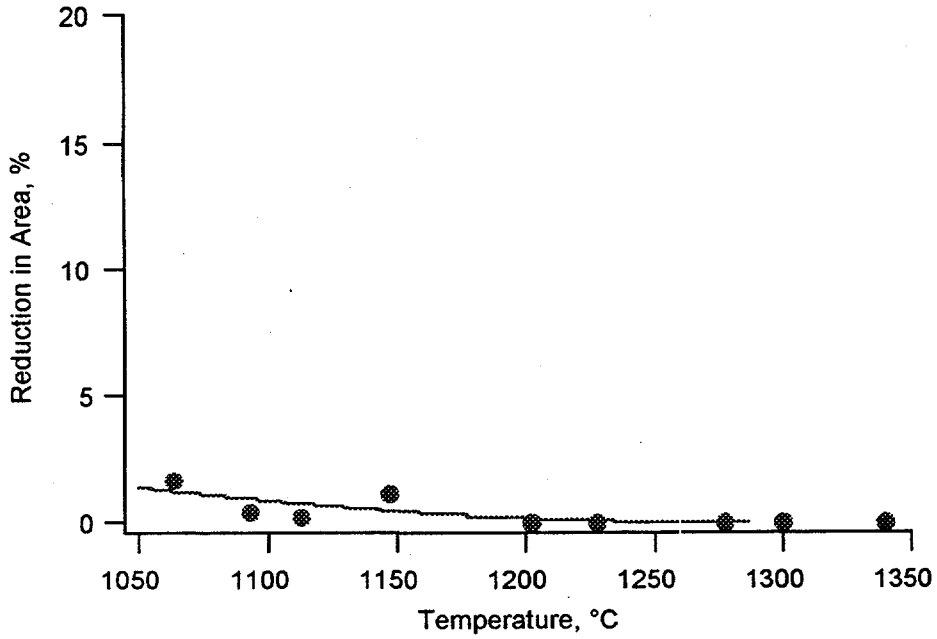

Figure 6 (contd.): Comparison of hot ductility measurements (upon cooling) for various alloys: (a) heat treated WSTC-4, (b) as-cast CMSX4, (c) heat treated CMSX4, (d) heat treated CM247DS, (e) heat treated CM247CC, (f) solutioned MarM002 (HT-1), (g) solutioned and aged MarM002 (HT-2).

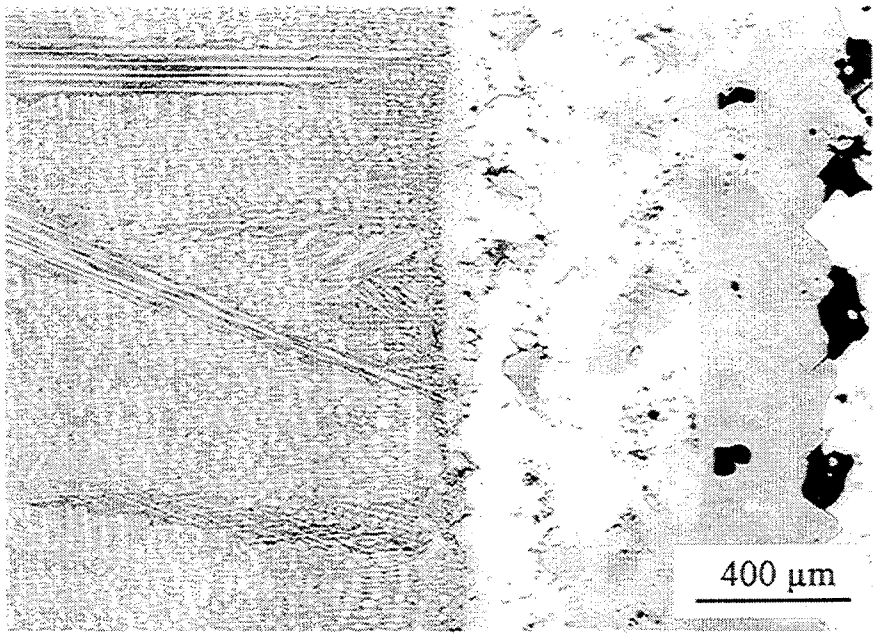

Figure 7: Fusion zone interface in a GTA weld on alloy CM247DS. The growth direction in the HAZ is aligned with the weld direction (vertical) and hence the HAZ along the interface is a single crystal. The growth of stray crystals in the fusion zone with different orientations is apparent.

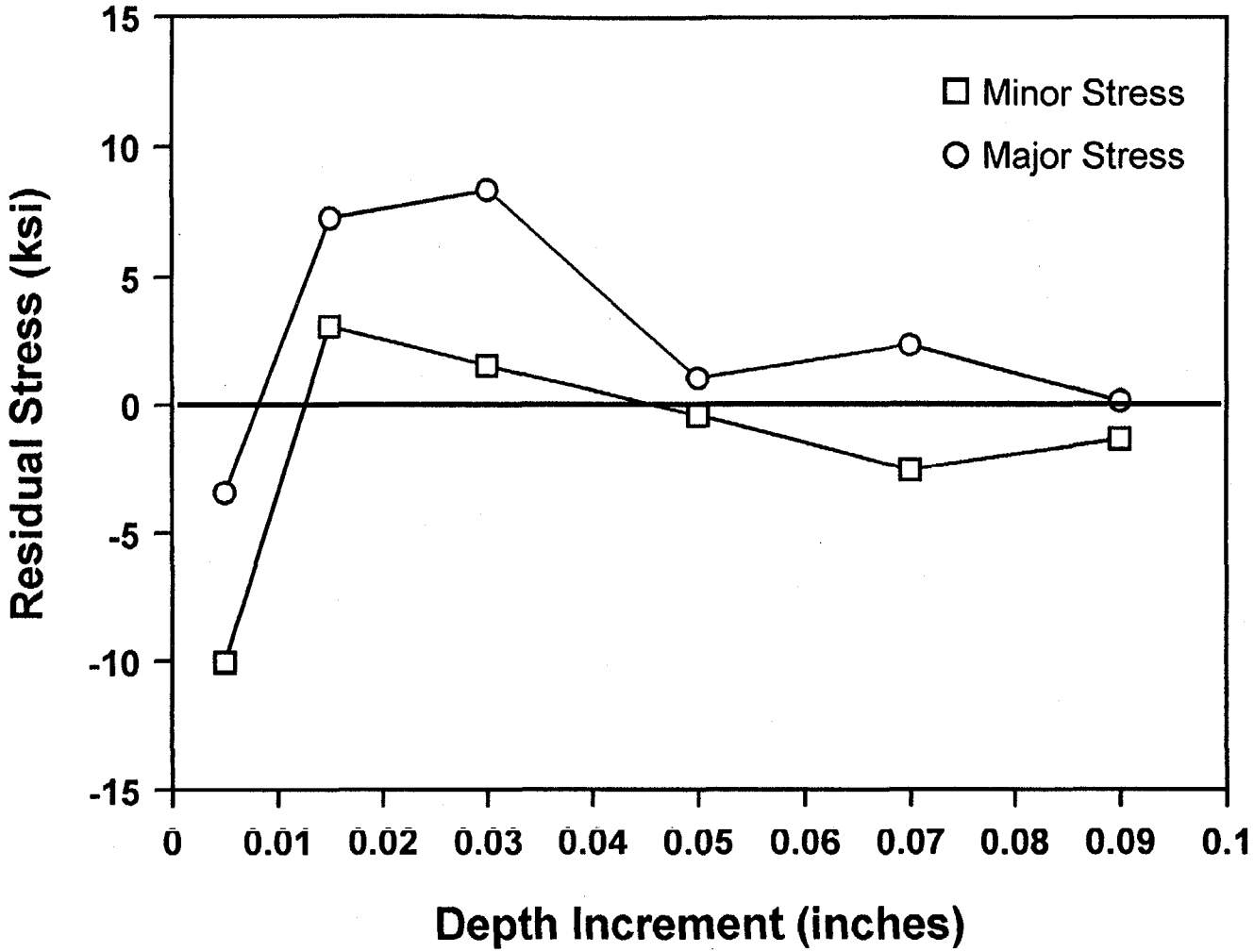

Figure 8: Plot of residual stress measured by hole drilling as a function of depth in as-cast CMSX4.

a)

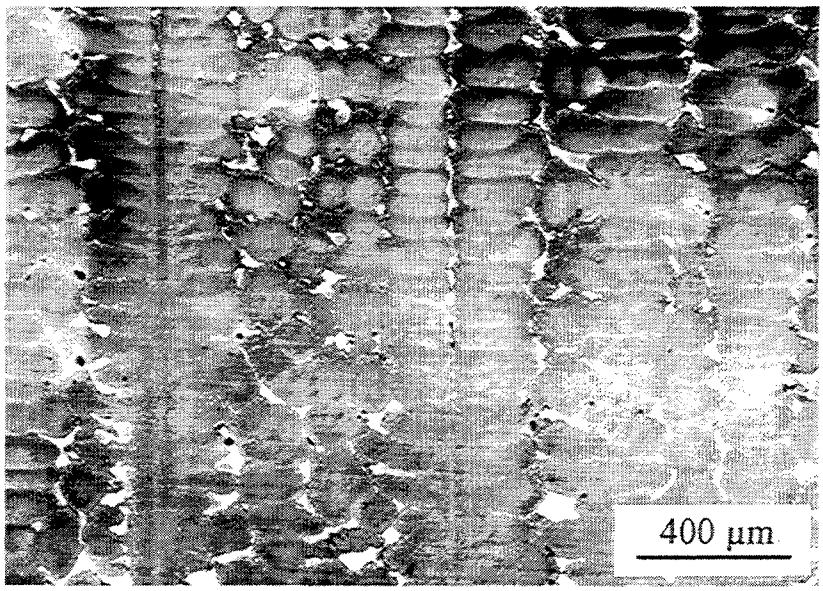

b)

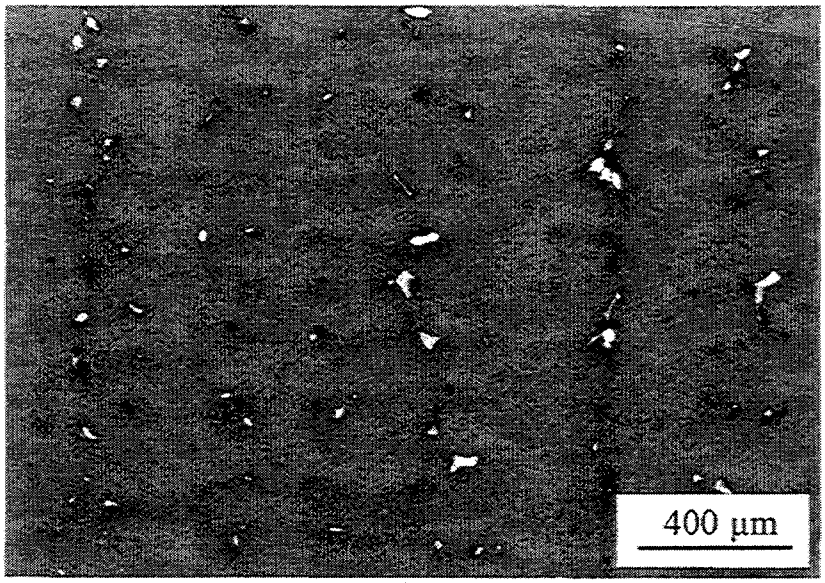

Figure 9: Optical micrographs of CMSX4 base material in the (a) as-cast and (b) heat treated conditions. The large interdendritic precipitates (likely to be γ') that form during solidification are still present after heat treating.

DISTRIBUTION

1-2. G. Wagner, Power Generation Technology Division, Westinghouse Electric Corporation, 4400 Alafaya Trail, MC 303, Orlando, FL 32826-2399
3-4. Laboratory Records (Office of Scientific and Technical Information, P.O. Box 62, Oak Ridge, TN 37831)
5. DOE, Oak Ridge Operations, P. O. Box 2001, Oak Ridge, TN 37831-6269
6. P. Angelini
7. E. E. Bloom
8. B. B. Bovee
9. R . A. Bradley
10. D. F. Craig
11. S. A. David
12. R. Ford
13. P. L. Gorman
14. H. W. Hayden, Jr.
15. A. J. Luffman
16. B. Painter
17. R. W. Reed
18. J. Shepherd
19. R. Steele
20. C. A. Valentine
21-22. J. M. Vitek
23. Document Reference Section
24. Laboratory Records - RC
25. ORNL Patent Section
26-27. Y-12 Central Files